Korean J. Chem. Eng., 38(11), 2294-2303 (2021)
DOI: 10.1007/s11814-021-0868-3

pISSN: 0256-1115
eISSN: 1975-7220

Facile synthesis of zero valent sulfur nanoparticles for catalytic detoxification of hexavalent chromium, cytotoxicity against microalgae and ultraviolet protection properties

Shama Sehar*,†, Layla Jassim Hazeem, Iffat Naz***, Abdul Rehman****, Wuyang Sun*****, Saleh S. Alhewairini******, Ali Salman Bin Thani**, Mohammad Salim Akhter*******, and Adnan Younis********,†**

*College of Science, University of Bahrain, P.O. Box 32038, Sakhir, Kingdom of Bahrain
**Department of Biology, College of Science, University of Bahrain, P.O. Box 32038, Sakhir, Kingdom of Bahrain
***Department of Biology, Deanship of Educational Services, Qassim University, Buraidah 51452, Qassim Kingdom of Saudi Arabia (KSA)
****Department of Microbiology, Kohat University of Science and Technology (KUST), Pakistan
*****School of Petrochemical Technology and Energy Engineering, Zhejiang Ocean University, Zhoushan, 316022, China
******Department of Plant Production and Protection, College of Agriculture and Veterinary Medicine, Qassim University, P.O. Box 6622, Buraidah 51452, Qassim, Kingdom of Saudi Arabia (KSA)
*******Department of Chemistry, College of Science, University of Bahrain, P.O. Box 32038, Sakhir, Kingdom of Bahrain
********Department of Physics, College of Science, University of Bahrain, P.O. Box 32038, Sakhir, Kingdom of Bahrain
(*Received 30 March 2021 • Revised 31 May 2021 • Accepted 13 June 2021*)

Abstract−Industrial effluents that contain various toxic substances have polluted our water and soil and posed major health issues. Thus, their removal or conversion to non-toxic products is highly crucial and desirable. This work emphasizes the synthesis of sulfur nanoparticles through precipitation method using anionic and cationic surfactants for exploring its catalytic efficiency in the photocatalytic reduction of hexavalent chromium Cr (VI). As-synthesized sulfur nanoparticles (SNPs) were physically characterized by UV-Vis absorption, scanning electron microscopy (SEM), Fourier transform infrared spectroscopy (FTIR), X-ray diffraction (XRD) and dynamic light scattering (DLS) measurements. The SNPs prepared using both surfactants have narrow size distribution with great homogeneity (50-80 nm). Moreover, excellent efficiency for Cr (VI) to Cr (III) reduction was recorded for SNPs. Besides, cytotoxicity analysis against microalgae *Picochlorum* sp. was analyzed and the SNPs showed no negative effect on algal growth and chlorophyll *a* concentration. Finally, the SNPs were found to provide excellent sunlight protection. Our results highlight that SNPs have great potential for the treatment of industrial wastewater with greater reproducibility. Moreover, they are equally effective against harmful sun rays and are suitable in different skin care products.

Keywords: Sulphur Nanoparticles, Reduction, Chromium, Wastewater, Cytotoxicity, Microalgae, Sun Protection Factor

INTRODUCTION

In recent years, nanomaterials have demonstrated exceptionally novel and multifunctional properties with unique characteristics through the manipulation of their size, shape, degree of aggregation, distribution and morphology [1-5]. They have been efficiently utilized for the degradation of harmful pollutants without generating additional byproducts. Nanoparticles are also being widely applied in diverse fields such as electroplating, sensors, drugs, gene delivery systems, biomedical and pharmaceutical applications [6-10]. Owing to large surface area, nanoparticles have served as excellent catalysts that exhibit photo redox reactions by generating holes and electrons upon irradiation from different light sources [11-14]. The catalytic activity of sulfur nanoparticles is also primarily determined by their size, where particle size and surface area have an inverse relationship. Therefore, it is critical to explore a robust, reliable and facile synthesis procedure that provides size-selective preparation of SNPs with narrow size distribution.

Hexavalent chromium, Cr (VI), is among the most toxic and nonbiodegradable heavy metal pollutants that exist in the forms of chromate (CrO_4^{2-}), dichromate ($Cr_2O_7^{2-}$) and CrO_3 [15]. Moreover, it possesses high oxidizing power, high solubility and mobility both in the environment and across the membranes in living organisms; it is mostly generated from various industries such as electroplating, tanning, dyes, paint and in wood preservation processes [16-21]. The discharge of this nonbiodegradable and toxic specie in freshwater streams and underground water reserves poses serious threats not only to existing ecological systems but also to humans, flora, fauna and aquatic systems due to its adverse carcinogenic and mutagenic effects [22-26]. Cr (VI) also causes severe inflammation, epithelial (skin) allergic reactions in human [27]. Therefore, it is of prime importance to either get rid of this toxic substance or

†To whom correspondence should be addressed.
E-mail: shamaseher@yahoo.com, adnaanyounis@yahoo.com

convert it to less toxic state, i.e., trivalent chromium (Cr (III)), so that its hazardous effects can be minimized. Contrary to Cr (VI), Cr (III) is an important micronutrient in humans that helps in sugar and lipid metabolism [28]. Hence, it is important to investigate the suitable nanomaterials which can efficiently convert Cr (VI) into Cr (III).

In past, sulfur nanoparticles and derivatives have been widely used as antimicrobial agents; however, there are few reports where SNPs have been exploited for biomedical applications as an anticancer agent [29]. On the other hand, toxicity, and low reactivity of sulfur nanoparticles (SNPs) could be the possible reasons for their limited applicability in drug delivery [30]. Therefore, the size modulation and homogeneity of SNPs could be an effective strategy to expand their applicability in various fields.

This work presents a facile one step, reproducible precipitation method for SNPs preparation with controlled size and homogeneity. By varying surfactant types (cetyltrimethylammonium bromide (CTAB) and sodium dodecyl sulfate (SDS), and their concentration, the final size of synthesized SNPs can be controlled. The formation of SNPs was confirmed by FTIR, UV-Vis absorption spectra and XRD studies. The morphology and size distribution of SNPs were determined by SEM and DLS studies. Afterwards, the prepared SNPs were subjected to various environmental and biological applications, such as photoreduction of toxic hexavalent Cr (VI) to less toxic Cr (III), cytotoxicity analysis against microalgae, *Picochlorum* sp., and to determine their sun protection factors. The prepared SNPs efficiently reduced toxic Cr (VI) content to less toxic Cr (III) state. Besides, SNPs exhibited excellent cytotoxicity response and broad-range sun protection factor through the spectrophotometric method.

MATERIAL AND METHODS

1. Chemicals

The chemicals used were sodium thiosulfate ($Na_2S_2O_3{\cdot}5H_2O$, 95%, Sigma-Aldrich), cetyltrimethylammonium bromide (CTAB, 99%, Sigma-Aldrich), sodium dodecyl sulfate (SDS, 99%, Sigma-Aldrich), malonic acid $CH_2(COOH)_2$ (99%, Sigma-Aldrich), potassium dichromate ($K_2Cr_2O_7$, 99%, Sigma-Aldrich), formic acid (HCOOH, 85%, Sigma-Aldrich). All the chemicals were analytical grade and used according to manufacturer's instructions.

2. Synthesis of Sulfur Nanoparticles (SNPs)

Sulfur nanoparticles were prepared through precipitation method. For typical synthesis, 50 ml of 0.8 M sodium thiosulfate ($Na_2S_2O_3{\cdot}5H_2O$) and 20 ml of 0.02 M of surfactants (CTAB and/or SDS) were dissolved in three separate beakers. All the mixtures were stirred

Table 1. Name and composition of as-synthesized sulfur nanoparticles

Name of samples	Composition of samples
SNP-1	0.8 M Sodium thiosulfate, 0.02 M SDS, 1 M Malonic acid.
SNP-2	0.8 M Sodium thiosulfate, 0.02 M SDS, 2 M Malonic acid.
SNP-3	0.8 M Sodium thiosulfate, 0.02 M CTAB, 1 M Malonic acid.
SNP-4	0.8 M Sodium thiosulfate, 0.02 M CTAB, 2 M Malonic acid.

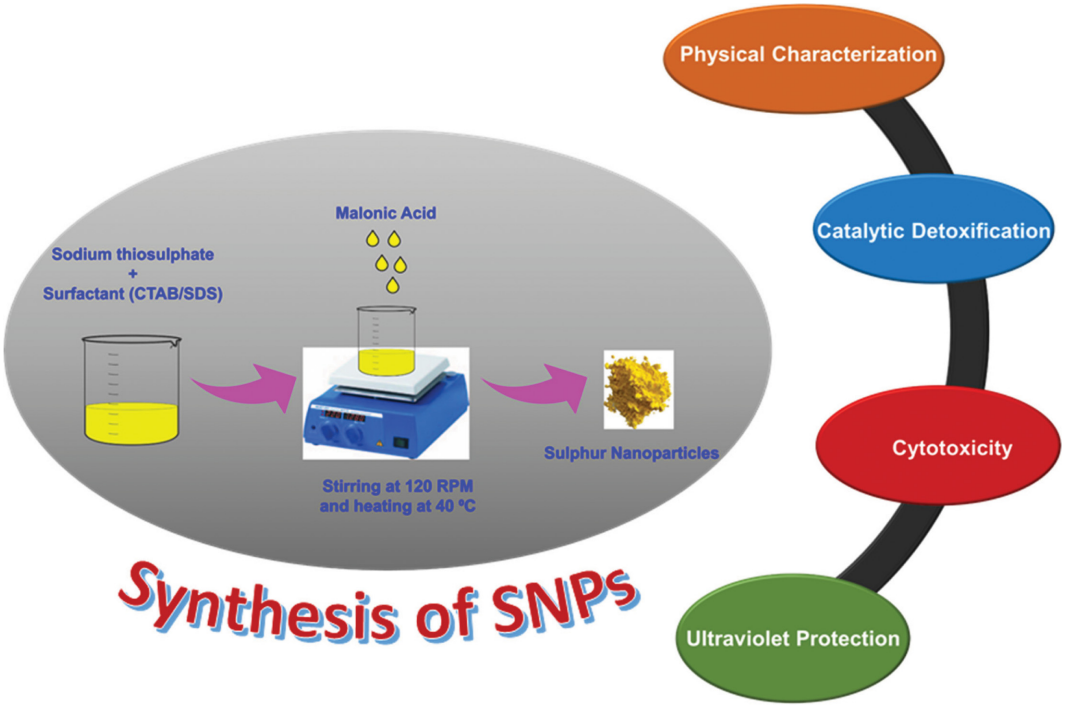

Fig. 1. Schematic representation of the entire study plan.

mechanically at 120 rpm and heated in a constant bath at 40 °C. After that, 40 ml of Malonic acid (1 M and/or 2 M) was added to the mixtures with continuous stirring for 40 min until yellow-colored precipitate was formed. The name of samples and their composition are shown in Table 1. The entire plan of study is schematically shown in Fig. 1.

3. Physical Characterization of Sulfur Nanoparticles (SNPs)

The preliminary characterization of SNPs was by UV-Vis spectroscopy (UV-1601 PC, Shimadzu, Japan) with the scanning range of 200-700 nm. The surface morphology of as-prepared SNPs was obtained using Nova SEM 230 operating at 200 kV. The phase composition and crystal structure of as-synthesized samples were analyzed through X-ray powder diffraction studies (Philips X'pert Multipurpose (MPD). The configurations used were: Cu Kα source (1.5418 Å), diffraction pattern ranging from 20°-80° for 2-Theta and 0.001°/s scan speed. To measure size distribution of as-prepared samples, DLS measurements were carried out with the help of dynamic light scattering photometer (ELS-Z, Otsuka Electronics, Japan). The as-prepared SNPs were subjected to Fourier transmission infrared spectroscopy (FTIR) analysis using KBr pellets method (Shimadzu, IRP Prestige-21). The spectra were measured in the wavelength range 500-4,000 cm^{-1}.

4. Conversion of Cr (VI) into Cr (III)

The catalytic behavior of as-synthesized samples was assessed during reduction of Cr (VI) to Cr (III) in order to estimate both the catalytic efficiency and reusability of SNPs. Formic acid (HCOOH) was used as a reducing agent. For this purpose, a mixture solution of water, $K_2Cr_2O_7$ and formic acid was prepared in a glass beaker in a water bath with a temperature of 50 °C, and then a piece of SNP-containing filter paper was immersed into the above mixture solution under gentle magnetic stirring. At each predetermined time interval, 0.5 mL of the aqueous solution was withdrawn and diluted to 1.0 mL for the analysis of transformation efficiency of Cr (VI) to Cr (III) using a UV-vis spectrometer (UV-1601 PC, Shimadzu, Japan) under simulated solar light irradiation (λ>400 nm) from tungsten lamp (150 mW/cm^{-2}). The pH of solution was maintained as 1.5 by addition of H_2SO_4. Similarly, a control was prepared in the same way except for the addition of nanoparticles. The entire methodology was repeated three times for each sample. The reduction of Cr (VI) into Cr (III) was calculated using the following equation [31].

$$\text{Reduction efficiency}\,(\%) = \left(\frac{1-C}{C_o}\right)\times 100$$

where C_o is the initial concentration and C is the concentration at a specific time interval, t.

The effect of concentration of catalyst on Cr reduction was studied at different concentrations of SNPs ranging from 0-25 mg/l.

5. Culturing of Microalgae *Picochlorum* sp. and Cytotoxicity Assay

The cytotoxicity assay was performed by using microalgae, *Picochlorum* sp. For this purpose, pure culture of microalgae, *Picochlorum* sp. was obtained from National Mariculture Centre, Ministry of Municipalities and Urban Planning, Kingdom of Bahrain. *Picochlorum* sp. was grown in 2 L Erlenmeyer flasks containing 1 L of sterilized f/2 medium (prepared with filtered seawater) maintained at pH 8 and incubated at 18 °C under illumination of approximately 100 µmol m^{-2} s^{-1} with 12 h light: 12 h dark cycle. Microalgae cells at exponential phase were incubated with 50 mgL^{-1} of (SNP-2 and SNP-4) at the above-mentioned growth conditions. Samples without nanoparticles were considered as control.

Cytotoxicity of microalgae *Picochlorum* sp. was assessed by various parameters, including viable cell concentration and determination of chlorophyll *a* content. Viable cell concentration of *Picochlorum* sp. (control) and *Picochlorum* sp. with SNP-2 and SNP-4 at 0 and 96 hours of incubation was recorded through MuseTM Cell analyzer (Millipore, USA). The Organization for Economic Cooperation and Development (OECD) 201 algal growth inhibition test guidelines, 1984 [32], were followed with some modifications.

For the determination of chlorophyll, *a* concentration, 30 mL of each treated algal culture was collected at 0 and 96 hours of incubation. Chlorophyll *a* was extracted using 90% acetone, and its concentration was measured using a spectrophotometer (Orion Aquameter 8000 UV-VIS spectrophotometer) by following UNESCO protocol [33].

A test of viable cell concentration and chlorophyll *a* concentration was performed using three replicates of each treated sample. The data is presented as mean and standard deviation (SD). Significant difference between treated and control groups was determined by one way Anova using minitab 14 software. All statistical analysis used the default 5% rejection level. Graphs were presented using Sigma Plot 13.

6. Determination of Sun Protection Factor (SPF)

To determine sun protection factor (SPF), 1 gram of as synthesized SNPs was dissolved in ethanol in a 100 mL volumetric flask. The mixture was then ultrasonicated for about 20 minutes. Afterwards, 5 mL of the prepared solution was dissolved in ethanol using a 50 mL volumetric flask. At the end, 5 mL of the solution was diluted in a 25 mL volumetric flask and absorption was measured from 290 to 320 nm at interval of 5 nm using spectrophotometry (Shimadzu 1601 model, Japan). Experiments were performed in triplicate and values were reported as mean±standard deviation. SPF factor for the synthesized nanoparticles was calculated by using the Mansur equation [34] as follows:

$$\text{SPF} = \text{CF}\sum_{290}^{320}\text{EE}(\lambda)\times\text{I}(\lambda)\times\text{Abc}(\lambda)$$

where, CF is correction factor (10 in this study), Σ is the sum of absorbance from 290 to 320 nm, EE(λ) is the erythema effect of the radiation at wavelength λ, I is the intensity of the sunlight at the wavelength λ, and Abc(λ) is the absorption of the wavelength λ by the tested solution. The value of EE(λ)×I(λ) is constant and was determined [35].

RESULTS AND DISCUSSION

1. Physical Characterization of Sulfur Nanoparticles

The surface morphology of as-prepared sulfur nanoparticles was investigated through scanning electron microscopy (SEM) and the results are depicted in Fig. 2. The anionic surfactant (SDS) showed a strong interaction between the micelles and the neighboring polymers chains; thus, an increased association of polymer chains

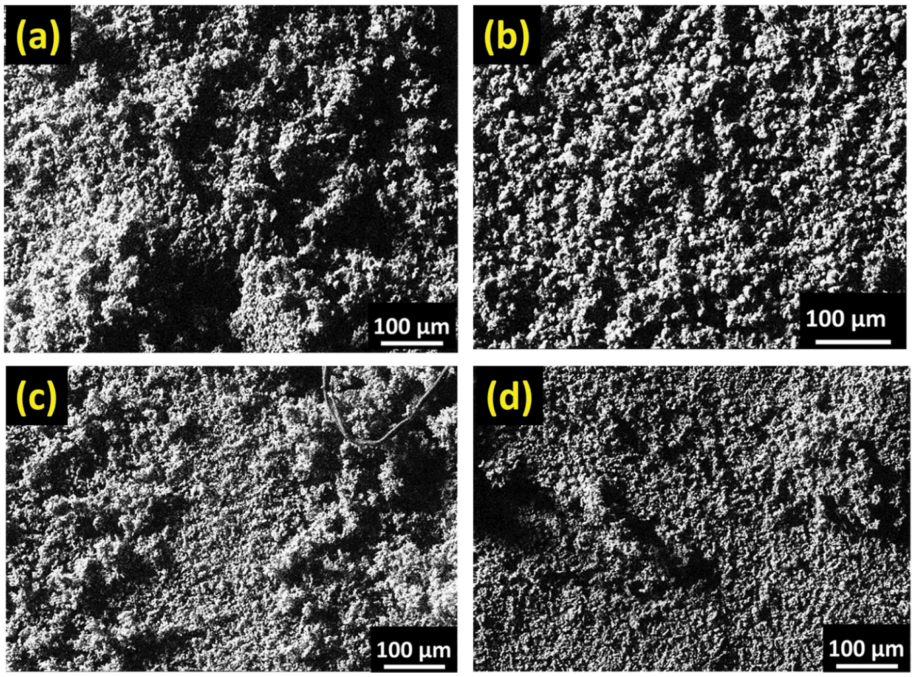

Fig. 2. Scanning electron microscopic images of as-synthesized samples, (a) SNP-1 (b) SNP-2 (c) SNP-3 (d) SNP-4.

is expected to form [36]. This may also increase the viscosity of solution, and narrow size distribution of SNPs with greater homogeneity is expected which is evident from Fig. 2(a) and 2(b). On the other hand, using CTAB as surfactant, the micelles may poorly interact with neighboring polymer chains with a possible decrease in solution viscosity. Therefore, a large variation in particle size (SNP-3 and SNP-4) with less homogeneity was observed as shown in Fig. 2(c) and 2(d). Moreover, higher surfactant concentration in the presence of higher Malonic acid can significantly lower the degree of agglomeration, and well dispersed SNPs were obtained as evident from Fig. 2(b) and 2(d).

It is noteworthy that the size of SNPs is dependent on both surfactant concentration and malonic acid, as higher concentration of each surfactant produces smaller NPs. The malonic acid acts as capping agent for stabilizing growth of SNPs as well as to protect them from agglomeration and loss of their surface features. Moreover, it may also help to control their morphology and roughness via electronic interaction, strong hydrogen-bonding, or weak van der Waals interactions [37]. Therefore, higher concentration of surfactants with the aid of higher concentration of malonic acid produces more homogeneous and smaller sized NPs as compared to their lower concentrations.

The FTIR spectra of SNP-2 and SNP-4 are depicted in Fig. 3. All characteristics peaks correspond to α-sulfur [38]. The absorption band from 3,600 to 3,300 cm^{-1} with peaks at 3,440 cm^{-1} could be assigned to -OH and -NH stretching [39]. The band at 2,800-3,000 cm^{-1} may be assigned to -CH stretching. The band at 1,600-1,750 cm^{-1} may be assigned to Amide I: C=O stretching mainly from proteins. The spectra peaks at 1,300-1,450 cm^{-1} may represent C=S stretching mainly from sulfur compounds [40]. The bands at 900-1,200 cm^{-1} may be assigned to C-O-C antisymmetric stretching, and bands at lower wavenumbers (500-800 cm^{-1}) may arise

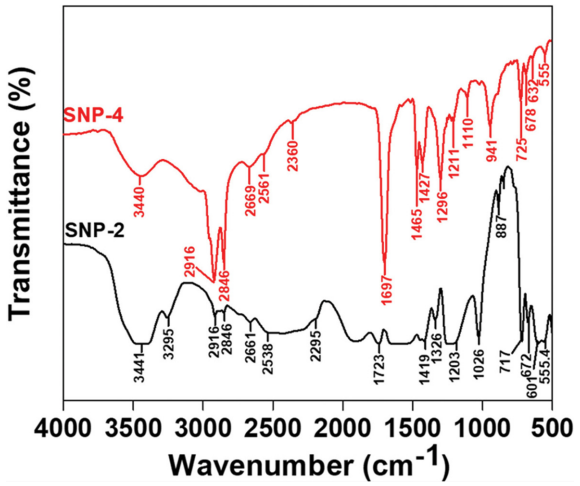

Fig. 3. The IR spectra of sulfur nanoparticles synthesized by using CTAB and SDS as surfactants.

from the C-S vibration due to the ethylene dioxy group [41]. A slight change in the peaks' intensity and positions was observed for SNP-4, which may be ascribed to different surfactants' absorption on the surface of SNP-4.

The crystalline structure of as-prepared SNPs was examined by X-ray diffraction (XRD) studies and corresponding spectra are depicted in Fig. 4. The major peaks located at 2-theta ~22.2, 27.4, 29.1, and 32.1 degrees are indexed as (222), (311), (206) and (313) planes of the cubic crystalline phase of SNPs with space group Fm-3m. The position and intensity of the prominent peaks matched well with the standard JCPDS 34-0394 of SNPs. Apart from the prominent peaks, there were many small peaks observed in the spectra, demonstrating the polycrystalline nature of as-prepared SNPs.

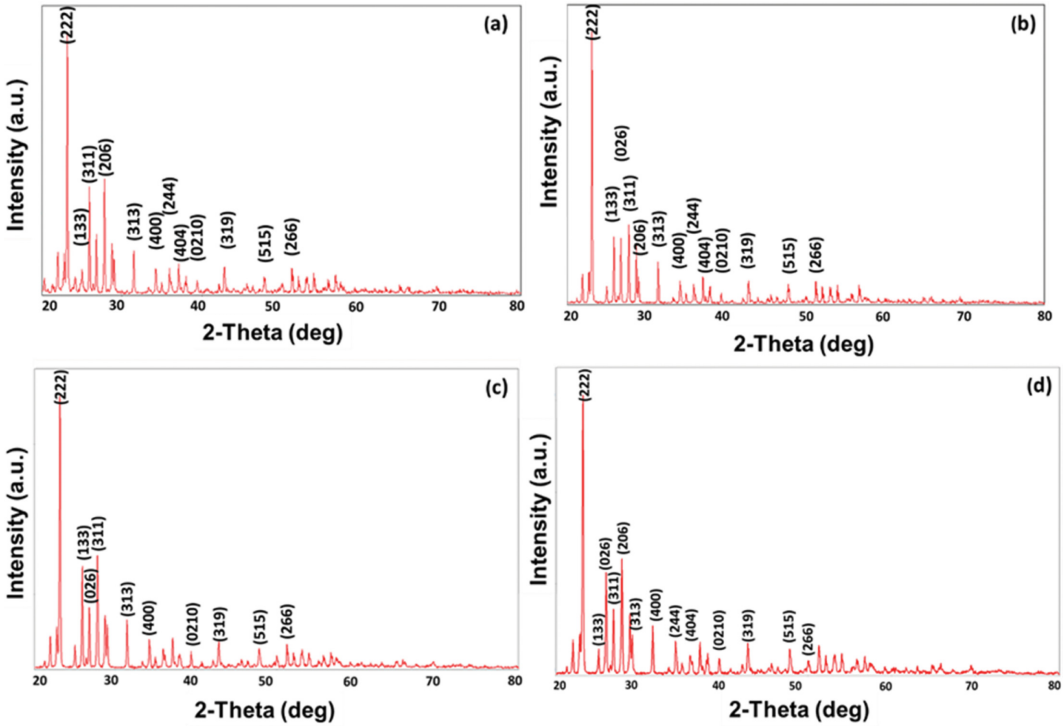

Fig. 4. X-ray diffraction spectra of prepared (a) SNP-1 (b) SNP-2 (c) SNP-3 (d) SNP-4.

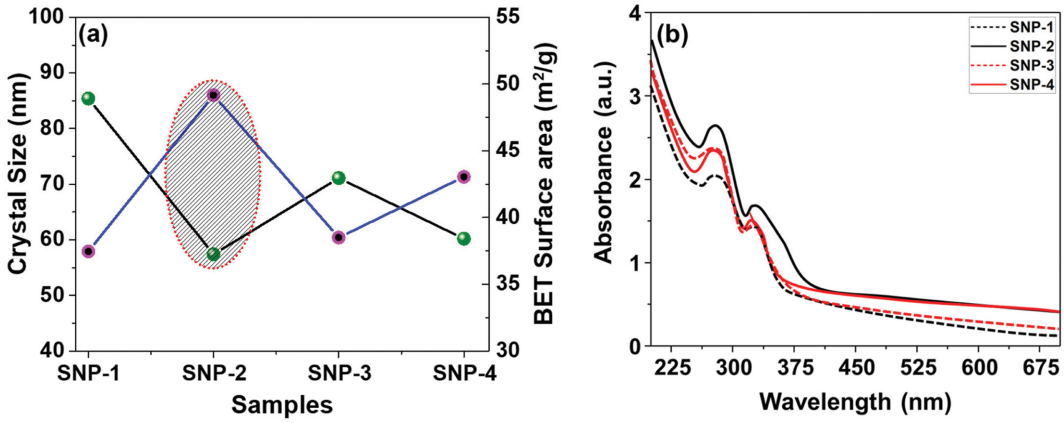

Fig. 5. (a) The variation of SNPs crystal size as determined by Debye-Scherrer equation using XRD spectra and corresponding BET surface area. (b) UV-Vis absorption spectrum of as-prepared SNPs.

From XRD data, the average particle sizes of the as-prepared SNPs were calculated using the Debye-Scherrer equation [42]:

$$D = \frac{K\lambda}{\beta \cdot \mathrm{Cos}\theta}$$

where, K, is the Scherrer constant, D is mean diameter of the particle, β is full width at half maximum of diffraction lines, λ is wavelength of X-ray source and θ is half diffraction angle.

The sample SNP-2 was found to exhibit the smallest crystal size among others as shown in Fig. 5(a). BET surface areas of all SNPs were calculated, and SNP-2 was found to exhibit the largest surface area (Fig. 5(a)) which further supports our diffraction results that smallest particles were exhibiting larger surface areas. In addition, the successful formation of sulfur nanoparticles was confirmed by UV-Vis absorption studies. Usually, the absorption spectra of sulfur nanoparticles are visible in the range of 250-300 nm and the maximum absorption can be found at around 280 nm [43]. Our results match well with the reported literature, and the maximum absorption of all SNPs was observed at around 274 nm as illustrated in Fig. 5(b) [44,45]. Another small shoulder peak was observed around 324 nm that may correspond to the conversion of b2→e3 transition energies [46].

The particle size distribution of as-prepared samples was measured through DLS and the results are depicted in Fig. 6. The size distribution of SNP-1 was found to be 75-105 nm, while for SNP-2, the sizes were estimated in the range of 40-75 nm. The sharp

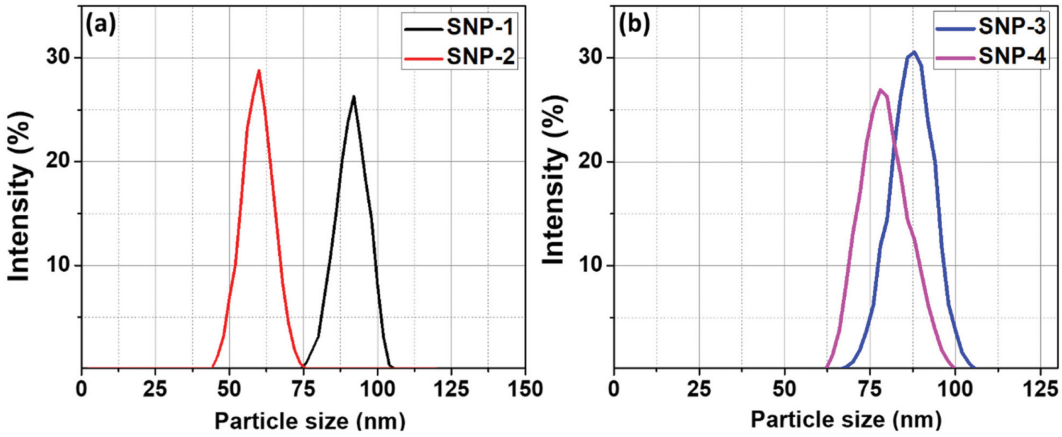

Fig. 6. Particle size distribution of sulfur nanoparticles measured through dynamic light scattering.

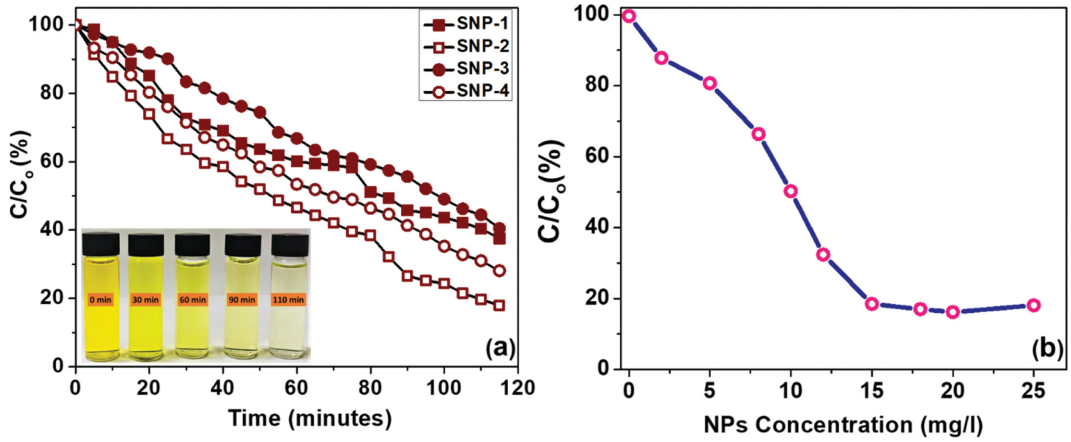

Fig. 7. (a) Catalytic degradation kinetics of Cr (VI) to Cr (III) in presence of SNP-1, SNP-2, SNP-3 and SNP-4. Photographs of the reaction mixture showing various stages of Cr (VI) reduction to Cr (III) (Inset of Fig. 7). (b) Investigations of reduction of Cr (VI) to Cr (III) efficiencies at various SNP-2 loading rates.

peaks for SNP-1 and SNP-2 indicate that both types of nanoparticles were narrowly distributed with peaks maxima were identified at 85.4 nm and 57.4 nm, respectively. Similarly, for SNP-3 and SNP-4, a narrow distribution of particle size was recorded and the average particle size for SNP-3 and SNP-4 was 71.1 nm and 60.2 nm, respectively.

Note that for the surfactant role it is not only critical to control particle size, in fact the concentration of malonic acid in the presence of surfactants is vital to obtain smaller particle sizes. However, the influence of malonic acid in the presence of SDS is more pronounced as compared to CTAB, as a significant reduction in particles size was obtained for the presence of SDS. Furthermore, the particle sizes obtained through DLS measurements slightly differ from the calculated crystal sizes by XRD measurements (calculations solely based on diffraction peaks and FWHM data). Besides, the trend through both measurements is the same and it is obvious that SNP-2 have smallest crystal size and exhibited highest surface area. Thus, it is likely that SNP-2 may facilitate better surface reactivity and demonstrates excellent catalytic responses.

2. Catalytic Conversion of Cr (VI) to Cr (III)

The catalytic conversion of Cr (VI) to Cr (III) in the presence of SNP-1, SNP-2, SNP-3 and SNP-4 was carried out at ambient conditions under sunlight without adjusting the pH of the reaction solution. Initially, 20 ppm of prepared sulfur nanoparticles was added to the reaction mixture and Cr (VI) conversion/reduction rate was monitored for 110 minutes. The reaction kinetics of the Cr (VI) was measured by recording absorbance at 350 nm as a function of time as shown in Fig. 7(a). The SNPs in the presence of Formic acid were very effective for the reduction of Cr (VI) to Cr (III). The maximum Cr (VI) to Cr (III) conversion was attained in the presence of SNP-2 (82%) followed by SNP-1 (69%), SNP-3 (62%) and SNP-4 (58%) over the period of reaction time as illustrated in Fig. 7(a). Moreover, an obvious fading of yellowish color of the dye solution by increasing reaction time was recorded as depicted in the inset of the Fig. 7(a). In contrast, no color change was observed for the dye solution without any sulfur nanoparticles, thus confirming the effectiveness of SNPs for Cr (VI) to Cr (III) reduction.

As SNP-2 exhibited superior reduction of Cr (VI) to Cr (III) in comparison to other synthesized SNPs, therefore further investigations were carried out for SNP-2. For instance, the reduction rate of Cr (VI) was recorded for different SNP-2 concentrations from

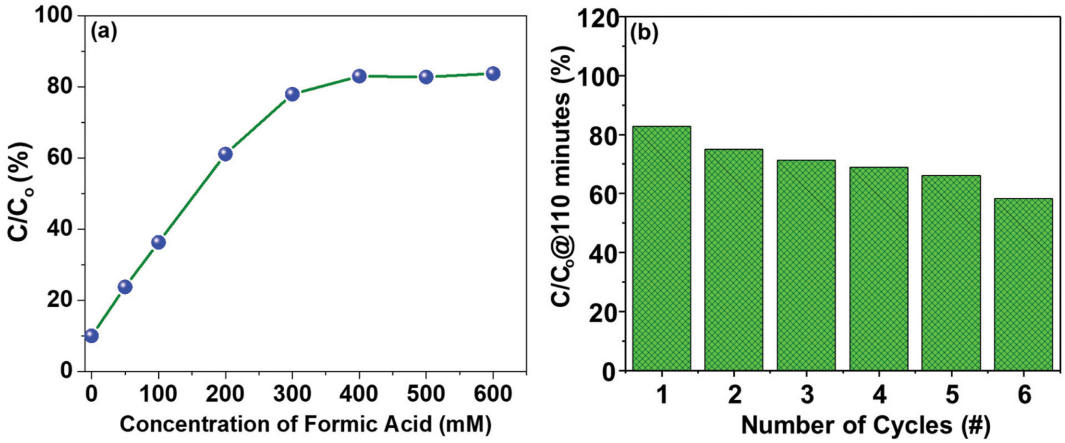

Fig. 8. (a) The influence of Formic acid for the conversion of Cr (VI) to Cr (III). (b) Cycling runs of reduction of Cr (VI) to Cr (III) after 120 min using SNP-2 for six successive cycles.

0-25 mg/l in dye solution. By increasing the SNP-2 concentration, the conversion rate of Cr (VI) to Cr (III) increased and the maximum efficiency was recorded at 15 mg/l with a conversion efficiency of 82% as illustrated in Fig. 7(b). This superior efficiency may be attributed to the availability of more active sites for Cr (VI) reduction by having high concentration of SNP-2. However, by further increasing SNP-2 concentration, relatively lower conversion rate with slightly reduced efficiencies was recorded. The availability of excessive SNP-2 may cause agglomeration, which may result in cluster formation. At this stage, charge separation rate decreases more than the charge recombination; thus lower efficiencies were obtained. Therefore, an optimum number of SNP-2 is required not only to avoid excessive catalyst dose, but also to guarantee effective absorption of light photons for efficient Cr (VI) reduction.

The influence of formic acid concentration on the catalytic activity of SNP-2 was also investigated (Fig. 8(a)) due to its low toxicity, high stability, and ease in storage (as a reducing agent). Also, formic acid provides acidic medium which is favorable for reduction of Cr (VI). The C/C$_o$ ratios were calculated for various formic acid concentrations at reaction time of 110 minutes in the presence of 15 mg/l of SNP-2. The reduction of Cr (VI) was increased by increasing formic acid concentration up to 400 mM, afterwards no prominent change in Cr (VI) reduction was observed. This indicates that the optimum concentration of formic acid is ~400 mM, which can provide maximum efficiency in the presence of 15 mg/l of SNP-2 as catalyst.

The recyclability and reusability of SNP-2 for the catalytic conversion of Cr (VI) to Cr (III) were also studied. After each cycle, the reaction mixture was centrifuged for 10 min at 5,500 rpm and washed with deionized water to extract SNP-2 for re-usability. The washed nanoparticles were then subjected to subsequent cycles under the same conditions. The conversion rate of Cr (VI) to Cr (III) (recorded at 110 minutes) was slightly decreased after each cycle; however, SNP-2 still demonstrated good reusability and reproducibility even after the sixth cycle (with more than 70% degradation efficiency) as shown in Fig. 8(b). This slight decline of photocatalytic efficiency may be attributed to the inevitable loss of photocatalysts during the recycle runs. The reduction in Cr conversion efficiency after each cycle can be attributed to (1) loss in particle yield during recovery process, (2) agglomeration of particles and/or surface passivation effects [47,48].

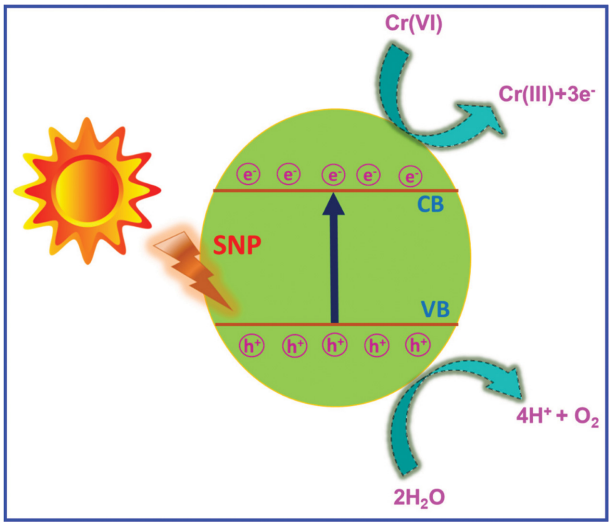

Fig. 9. Schematics of the proposed mechanism for photoreduction of Cr (VI) to Cr (III) with the help of sulfur nanoparticles.

3. Proposed Mechanism for Sunlight Induced Photocatalytic Conversion of Cr (VI) to Cr (III)

The possible underlying mechanism for photocatalytic conversion of Cr (VI) to Cr (III) in the presence of sulfur nanoparticles is illustrated in Fig. 9. The influence of sunlight triggers the generation of both electrons and holes in the conduction band (CB) and valence band (VB) of sulfur nanoparticles as represented by Eq. (1). These photoinduced electrons in VB then react with water (H_2O) to generate highly reactive (H^+) and O_2 as shown in Equation (2) [49]. Next, these photogenerated H^+ and electrons may react with the Cr (VI), located in the surrounding of SNPs and photo reduce toxic Cr (VI) to less toxic Cr (III) as shown in Eq. (3).

$$(\text{Sulphur NP}) + h\nu \rightarrow h^+ + e^- \quad (1)$$

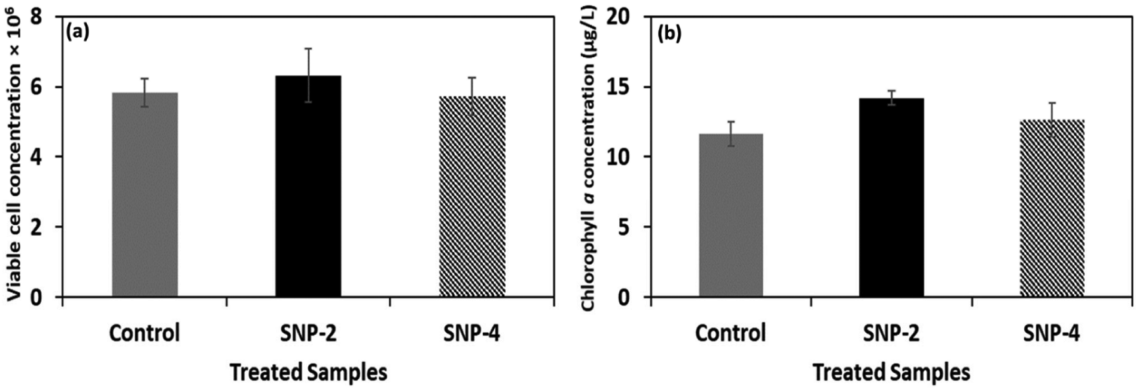

Fig. 10. Viable cell concentration (a) and chlorophyll *a* (b) concentration (μg/L) in control and treated samples after 96 hours of incubation.

$$2H_2O+4h^+ \rightarrow O_2+4H^+ \quad (2)$$

$$Cr_2O_7^{2-}+14H^++6e^- \rightarrow 2Cr(III)+7H_2O \quad (3)$$

The nanosized sulfur with a bandgap of about ~3.8 eV under visible light can absorb photons to separate electrons in the conduction band (CB) and holes in the valance band (VB). Usually, at lower pH value, the surface of inorganic NPs becomes positively charged. As the main chemical specie for Cr (VI) at low pH (~3) is $HCrO_4^-$, an electrostatic interaction (attraction) between nanosized sulfur and $HCrO_4^-$ may become established and adsorbed Cr (VI) on the surface of SNPs that can immediately react with electrons and get reduced to Cr (III). The presence of formic acid captures hydroxyl radicals ($HO^{\bullet}$), which were generated by holes and OH^- ions to produce reactive carbon dioxide ($^{\bullet}CO_2$). Thus, formic acid can facilitate electron-hole separation, which is advantageous to the photocatalytic activity of SNPs to produce reactive radicals ($^{\bullet}CO_2$) for efficient Cr (VI) to Cr (III) reduction [50].

4. Cytotoxicity Assay

After establishing the superiority of SNP-2 and SNP-4 over other SNPs in our previous measurements, the cytotoxicity of SNP-2 and SNP-4 for *Picochlorum* sp., was assessed through various parameters, such as viable cell concentration and chlorophyll, *a* concentration. Viable cell concentration of control (*Picochlorum* sp., without nanoparticles) and *Picochlorum* sp., with SNP-2 and SNP-4 is illustrated in Fig. 10(a). No significant difference between control and treated nanoparticles was observed. The inhibition rate was calculated with the tested SNPs and it was found that SNP-4 showed only 2% inhibition rate compared to the control samples. In contrast, SNP-2 showed a higher concentration of viable cells compared to the control.

The algae used in the present study belong to phytoplankton, and photosynthesis, which is an important physiological process of algae. Algae photosynthesis could be affected by the shading effect due to the adsorption of NPs on the surface of algal cells [51,52]. Pigment concentration, chlorophyll *a* in particular can be affected by the shading effect caused by NPs, which might reduce the algae absorption of light, thus inhibiting the photosynthesis process [53, 54]. The concentration of chlorophyll *a* at 96 hours of incubation is illustrated in Fig. 10(b). Overall, an increase in concentration of chlorophyll *a* was observed in control and treated samples. The concentration of chlorophyll *a* increased up to 22% in microalgae treated with SNP-2 as compared to 6% in microalgae treated with SNP-4. However, 52% increase in chlorophyll *a* concentration was observed in control samples. Regardless of the general increase in chlorophyll *a* concentration in all samples (control and treated samples), there was a significant difference between control and the treated samples ($p<0.05$). The tested concentration (50 mg/L) of SNPs did not lead to a negative effect on algae growth and chlorophyll *a* concentration. Similar results were found when SNPs at 100-400 ppm were used with the plant (*Cucurbita pepo*) and found to have a positive effect on several parameters (i.e., number of leaves, number of branches, height per plant and stem diameter) [55]. In comparison, other types of NPs (e.g., Ag, CuO, TiO_2 and ZnO) were found to have a toxic effect on different species of microalgae by causing a damage in chloroplast, [56] reduction in the concentration and growth of chlorophyll [57-59] and decrease in photosynthetic efficiency [60]. Additional chronic investigation using different concentrations of SNPs and different cell lines and organisms is required to draw a better conclusion.

5. Determination of Sun Protection Factor (SPF)

Sun protection factor (SPF) is the measurement of solar energy

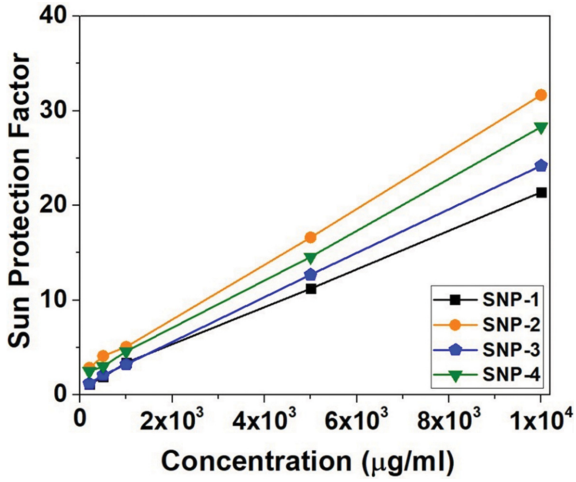

Fig. 11. Sun protection factor (SPF) of as-synthesized nanoparticles SNP-1, SNP-2, SNP-3 and SNP-4.

(UV radiation) that is required to produce sunburn effect on protected skin (presence of sunscreen) comparable to the amount of solar energy required to produce sunburn on unprotected skin (absence of sunscreen). SPF factor can be calculated both by clinical and spectrophotometric analysis. However, clinical trials are much more time-consuming than spectrophotometric analysis, and there is no significant difference in results by following both methods [35]. Therefore, in this study, SPF factor was measured through spectrophotometric analysis using the Mansur equation [34].

Higher values of SPF were recorded for higher SNPs concentration. The highest protection factor at concentration of 1×10^4 μg/ml was recorded as 31.66 for SNP-2 compared to 21.39, 24.19 and 28.28 for SNP-1, SNP-3 and SNP-4, respectively, as shown in Fig. 11. The recorded SPF of SNP-2 in our study is comparable to the best reported oxide nanoparticles CeO_2, ZnO_2 and TiO_2, respectively [61-64]. Thus, we can infer that SNPs are potentially active materials for providing protection against UV to human skin.

CONCLUSIONS

We report the synthesis of sulfur nanoparticles by one step precipitation method using anionic (SDS) and cationic surfactants (CTAB) by varying concentration of malonic acid. The as-synthesized SNPs were physically characterized through various techniques and investigated for environmental and biological applications. The use of cationic surfactant with high concentration of malonic acid greatly influences the size and dispersion of SNPs, where SNP-2 exhibited smaller size and better homogeneity. All synthesized SNPs exhibited excellent photoconversion of Cr (VI) to Cr (III); however, the best photoconversion efficiency was recorded for SNP-2 (82%) at catalyst concentration of 15 mg/l. Cytotoxic studies revealed that SNPs (SNP-2 in particular) are environment friendly and do not have any harmful impact on microalgae, *Picochlorum* sp., and its chlorophyll *a* content. Moreover, all synthesized SNPs were proven to provide protection against harmful sun rays, as SPF was found to be more than 15 with highest SPF of 31.66 recorded for SNP-2. Overall, this study advocates that zerovalent sulfur nanoparticles can have wide-ranging applications in environment, biomedical as well as in skin care products.

AUTHOR CONTRIBUTIONS

Shama Sehar: Conceptualization, data curation, formal analysis, investigation, methodology, resources, validation, visualization, writing- reviewing and editing. **Layla Jassim Hazeem:** formal analysis, investigation, methodology, validation, writing- reviewing and editing. **Iffat Naz:** reviewing and editing. **Abdul Rehman:** validation, reviewing and editing. **Wuyang Su:** revised this manuscript to develop the writing in scientific discussion. **Saleh S. Alhewairini:** revised this manuscript to develop the writing in scientific discussion. **Ali Salman Bin Thani:** revised this manuscript to develop the writing in scientific discussion. **Mohammad Salim Akhter:** methodology, resources, validation, visualization, reviewing and editing. **Adnan Younis:** Conceptualization, formal analysis, methodology, project administration, resources, supervision, visualization, writing-reviewing and editing.

CONFLICT OF INTEREST

All the authors declare no competing and financial interests.

ACKNOWLEDGEMENTS

We are indebted to Ms. Maryam Jaffar and Ms. Muneera Hayat from Department of Chemistry of University of Bahrain for providing assistance in carrying out XRD, SEM and FTIR experiments.

REFERENCES

1. M. C. Daniel and D. Astruc, *Chem. Rev.*, **104**, 293 (2004).
2. A. Younis, D. Chu, C. M. Li, T. Das, S. Sehar, M. Manefield and S. Li, *Langmuir*, **30**, 1183 (2014).
3. A. Younis, D. Chu, Y. V. Kaneti and S. Li, *Nanoscale*, **8**, 378 (2016).
4. S. Sehar, I. Naz, A. Rehman, W. Sun, S. S. Alhewairini, M. N. Zahid and A. Younis, *Appl. Organomet. Chem*., **35**, e6069 (2021).
5. A. Younis, *Physica. E. Low Dimens. Syst. Nanostruct.*, **126**, 114475 (2021).
6. S. He, Z. Guo, Y. Zhang, S. Zhang, J. Wang and N. Gu, *Mater. Lett.*, **61**, 3984 (2007).
7. D. R. Bhumkar, H. M. Joshi, M. Sastry and V. B. Pokharkar, *Pharm. Res.*, **24**, 1415 (2007).
8. A. Younis, D. Chu and S. Li, *J. Mater. Chem. C.*, **2**, 10291 (2014).
9. A. Younis, L. Zhang, D. Chu and S. Li, *Appl. Phys. Lett.*, **108**, 033506 (2016 b).
10. F. T. Thema, E. Manikandan, A. Gurib-Fakim and M. Maaza, *J. Alloys Comp.*, **657**, 655 (2016).
11. D. N. Li, F. Q. Shao, J. J. Feng, J. Wei, Q. L. Zhang and A. J. Wang, *Mater. Chem. Phys.*, **205**, 64 (2018).
12. L. Y. Hu, L. X. Chen, M. T. Liu, A. J. Wang, L. J. Wu and J. J. Feng, *J. Colloid Interface Sci.*, **493**, 94 (2017).
13. A. Younis, A. Chu, A. H. Shah, H. Du and S. Li, *ACS Appl. Mater. Interfaces*, **9**, 1585 (2017).
14. S. Sehar, I. Naz, I. Perveen and S. Ahmed, *Korean J. Chem. Eng.*, **36**, 56 (2019).
15. X. Guo, G. T. Fei, H. Su and L. De Zhang, *J. Phys. Chem. C*, **115**, 1608 (2011).
16. S. Avudainayagam, M. Megharaj, G. Owens, R. Kookana, D. Chittleborough and R. Naidu, in *Chemistry of chromium in soils with emphasis on tannery waste sites*, Ware G. W. Eds., Springer, New York, NY (2003).
17. C. Desai, K. Jain and D. Madamwar, *Bioresour. Technol.*, **99**, 6059 (2008).
18. Z. Lu, X. Ouyang, W. Zhang and F. Lu, *Appl. Mech. Mater.*, **295**, 74 (2013).
19. K. Jain, C. Desai and D. Madamwar, *Bacterial interaction with chromium and strategies for remediation of hexavalent chromium pollution*, in: Microbe Interaction and Bioremediation: Principal and Applications for Toxic Metals, CRC Press Taylor and Francis Group, Boca Raton (2017).
20. M. A. Ahmed, A. T. Elsir, F. Mohammed, H. A. Elbushra, S. Tawer and N. Eassa, *MRS Adv.*, **3**, 42 (2018).

21. L. W. Duresa, D. H. Kuo, K. E. Ahmed, M. A. Zeleke and H. Abdullah, *New J. Chem.*, **43**, 8746 (2019).
22. A. S. Ellis, T. M. Johnson and T. D. Bullen, *Science*, **295**, 2060 (2002).
23. A. Chiu, X. L. Shi, W. K. P. Lee, R. Hill, T. P. Wakeman, A. Katz, B. Xu, N. S. Dalal, J. D. Robertson, C. Chen, N. Chiu and L. Donehower, *J. Environ. Sci. Health C. Environ. Carcinog. Ecotoxicol. Rev.*, **28**, 188 (2010).
24. M. S. Khan, A. Zaidi and P. A.Wani, in *Chromium-plant-growth-promoting rhizobacteria interactions: Toxicity and management*, A. Zaidi, P. A. Wani and M. S. Khan, Eds., Springer, Vienna (2012).
25. H. Abdullah and D. H. Kuo, *ACS Appl. Mater. Interfaces*, **7**, 26941 (2015).
26. H. Zhao, G. Zhang, S. Chong, N. Zhang and Y. Liu, *Ultrason. Sonochem.*, **27**, 474 (2015).
27. C. Adam, J. Wohlfarth, M. Haußmann, H. Sennefelder, A. Rodin, M. Maler, S. F. Martin, M. Goebeler and M. Schmidt. *J. Invest. Dermatol.*, **137**, 367 (2017).
28. S. Nezar, Y. Cherifi, A. Barras, A. Addad, E. Dogheche, N. Saoula, N. A. Laoufi, P. Roussel, S. Szunerits and R. Boukherroub, *Arab. J. Chem.*, **12**, 215 (2019).
29. S. R. Choudhury, S. Roy, A. Goswami and S. Basu, *J. Antimicrob. Chemother.*, **67**, 1134 (2012).
30. Z. Faten, H. Mustafa and A. L. D. Muayad, *J. Microb. Biochem. Technol.*, **10**, 59 (2018).
31. S. Valizadeh, M. H. Rasoulifard and M. S. S. Dorraji. *Korean J. Chem. Eng.*, **33**, 481 (2016).
32. Organization for Economic Cooperation and Development. Guideline for testing of chemicals. No. 201. Alga growth inhibition test. Paris, France (1984).
33. F. C. Vohra, *Determination of photosynthetic pigment in seawater. Monographs on oceanographic methodology*, UNESCO, France (1966).
34. M. M. Donglikar and S. L. Deore, *Pharmacogn. J.*, **8**, 171 (2016).
35. R. M. Sayre and H. S. Black, *J. Photochem. Photobiol. B.*, **12**, 83 (1992).
36. D. Ramimoghadam, M. Z. B. Hussein, Y. H. Taufiq-Yap, *Int. J. Mol. Sci.*, **13**, 13275 (2012).
37. G. A. El-Nagar, R. M. Sarhan, A. Abouserie, N. Maticiuc, M. Bargheer, I. Lauermann and C. Roth, *Sci. Rep.*, **7**, 12181 (2017).
38. H. L. Strauss and J. A. Greenhouse, *Elemental sulfur chemistry and physics*, Meyer, B. Interscience Publishers, New York (1965).
39. S. Shankar and J. W. Rhim, *Food Hydrocoll.*, **82**, 116 (2018).
40. K. Khairan, Zahraturriaz and Z. Jalil, *Rasayan J. Chem.*, **12**, 50 (2019).
41. H. J. Shin, S. S. Jeon and S. S. Im, *Synth. Met.*, **161**, 1284 (2011).
42. U. Holzwarth and N. Gibson, *Nat. Nanotechnol.*, **6**, 534 (2011).
43. R. M. Tripathi, R. P. Rao and T. Tsuzuki, *RSC Adv.*, **8**, 36345 (2018).
44. R. G. Chaudhuri and S. Paria, *J. Colloid. Interface Sci.*, **354**, 563 (2011).
45. P. Suryavanshi, R. Pandit, A. Gade, M. Derita, S. Zachino and M. Rai, *Lwt-Food Sci. Technol.*, **81**, 188 (2017).
46. N. V. Richardson and P. Weinberger, *J. Electron. Spectros. Relat. Phenomena*, **6**, 109 (1975).
47. Z. Farooqi, M. W. Akram, R, Begum, W. Wu and A. Irfan, *J. Hazard. Mater.*, **402**, 123535 (2021).
48. R. M. Tripathi and S. J. Chung, *Sci. Rep.*, **10**, 640 (2020).
49. J. Wu, B. Liu, Z. Ren, M. Ni, C. Li, Y. Gong, W. Qin, Y. Huang, C. Q. Sun and X. Liu, *J. Colloid. Interface Sci.*, **517**, 80 (2018).
50. J. B. Islam, M. Furukawa, I. Tateishi, H. Katsumata and S. Kaneco, *Chem. Eng.*, **3**, 33 (2019).
51. E. Navarro, A. Baun, R. Behra, N. B. Hartmann, J. Filser, A. J. Miao, A. Quigg, P. H. Santschi and L. Sigg, *Ecotoxicology*, **17**, 372 (2008).
52. F. Wang, W. Guan, L. Xu, Z. Ding, H. Ma, A. Ma and N. Terry, *Appl. Sci.*, **9**, 1534 (2019).
53. F. Perreault, A. Oukarroum, S. P. Melegari, W. G. Matias and R. Popovic, *Chemosphere*, **87**, 1388 (2012).
54. X. Chen, C. Zhang, L. Tan and J. Wang, *Environ. Pollut.*, **236**, 454 (2018).
55. N. Salem, L. Albanna, A. Awwad, Q. Ibrahim and A. Abdeen, *J. Agric. Sci.*, **8**, 188 (2016).
56. V. Iswarya, M. Bhuvaneshwari, S. A. Alex, S. Iyer, G. Chaudhuri, P. T. Chandrasekaran, G. M. Bhalerao, S. Chakravarty, A. M. Raichur, N. Chandrasekaran and A. Mukherjee, *Aquat. Toxicol.*, **161**, 154 (2015).
57. C. Wei, Y. Zhang, G. Jing, H. Bing, Y. Xu and J. Yuan, *J. Environ. Sci.*, **22**, 155 (2010).
58. I. M. Sadiq, S. Pakrashi, N. Chandrasekaran and A. Mukherjee, *J. Nanoparticle Res.*, **13**, 3287 (2011).
59. S. Zheng, Q. Zhou, C. Chen, F. Yang, Z. Cai, D. Li, Q. Geng, Y. Feng and H. Q. Wang, *Sci. Total Environ.*, **660**, 1182 (2019).
60. D. M. Barreto and A. T. Lombardi, *Water Air Soil Pollut.*, **227**, 450 (2016).
61. A. Miri, M. Darroudi and M. Sarani, *Appl. Organomet. Chem.*, **34**, e5308 (2020).
62. V. Srikant and D. R. Clarke, *J. Appl. Phys.*, **83**, 5447 (1998).
63. S. Valencia, J. M. Marín and G. Restrepo, *Open Mater. Sci. J.*, **4**, 9 (2009).
64. A. Younis and A. Loucif, *Ceram. Int.*, **47**, 15500 (2021).